

Virgo: Cluster-level Matrix Unit Integration in GPUs for Scalability and Energy Efficiency

Hansung Kim*

University of California, Berkeley
Berkeley, California, USA
hansung_kim@berkeley.edu

Ruohan Richard Yan*

University of California, Berkeley
Berkeley, California, USA
yrh@berkeley.edu

Joshua You

University of California, Berkeley
Berkeley, California, USA
jyou12@berkeley.edu

Tieliang Vamber Yang[†]

NVIDIA Corporation
Santa Clara, California, USA
vamberry@nvidia.com

Yakun Sophia Shao

University of California, Berkeley
Berkeley, California, USA
ysshao@berkeley.edu

Abstract

Modern GPUs incorporate specialized matrix units such as Tensor Cores to accelerate GEMM operations, which are central to deep learning workloads. However, existing matrix unit designs are tightly coupled to the SIMT core, restricting operation size due to register file capacity and bandwidth constraints. Such a limitation in scalability makes it difficult to simultaneously improve compute throughput and energy efficiency in GPUs.

To address this challenge, we propose *Virgo*, a GPU microarchitecture that integrates dedicated matrix units at the *SIMT core cluster* level. By decoupling the matrix unit from the SIMT core, Virgo eliminates scalability constraints imposed by the core microarchitecture. Consequently, Virgo increases operation granularity at the hardware level, reducing energy overhead from core instruction processing. Physical disaggregation also enables a unified matrix unit design and offloading both operand and accumulator accesses from the register file, improving data reuse and energy efficiency. Furthermore, this disaggregation supports efficient concurrent execution of the SIMT core and matrix unit, optimizing mapping for fused DNN workloads. Our evaluations using synthesizable RTL demonstrate that Virgo achieves 67.3% and 24.2% reduction in on-chip active power consumption, compared to the baseline Ampere-style and Hopper-style core-coupled designs.

CCS Concepts: • Computer systems organization → Multicore architectures; Single instruction, multiple data; Systolic arrays; • Hardware → Power and energy.

*Both authors contributed equally to this work.

[†]Work done while at UC Berkeley.



This work is licensed under a Creative Commons Attribution 4.0 International License.

ASPLOS '25, Rotterdam, Netherlands

© 2025 Copyright held by the owner/author(s).

ACM ISBN 979-8-4007-1079-7/2025/03

<https://doi.org/10.1145/3676641.3716281>

Keywords: GPUs, Microarchitecture, Accelerators, Scalability, Power and Energy, Machine Learning

ACM Reference Format:

Hansung Kim, Ruohan Richard Yan, Joshua You, Tieliang Vamber Yang, and Yakun Sophia Shao. 2025. Virgo: Cluster-level Matrix Unit Integration in GPUs for Scalability and Energy Efficiency. In *Proceedings of the 30th ACM International Conference on Architectural Support for Programming Languages and Operating Systems, Volume 2 (ASPLOS '25), March 30-April 3, 2025, Rotterdam, Netherlands*. ACM, New York, NY, USA, 18 pages. <https://doi.org/10.1145/3676641.3716281>

1 Introduction

In recent years, the computational capability of GPUs has surged at an unprecedented rate, driven by the demand of emerging large-scale deep learning applications such as large language models [9, 19, 36]. To better meet these application demands, modern GPU architectures have increasingly incorporated specialized matrix units, such as NVIDIA Tensor Cores [13] and AMD Matrix Cores [1]. These units accelerate GEMM operations in deep learning workloads with significantly higher compute efficiency than the traditional general-purpose SIMD units.

As the demand for higher compute capabilities grows, so too has the scale of integration of dedicated matrix units: the number of FLOPS achieved by Tensor Cores has increased eight-fold from Volta to Hopper, over the past five years [13, 16]. Beyond FLOPS, power and energy have become increasingly important concerns for modern GPU workloads. Namely, deep learning applications are known to be highly energy-intensive workloads on GPUs [24]. GPUs are also often power-limited; datacenters over-provision GPU resources, leading to frequent throttling to meet the power budget, which in turn compromises performance [8, 31–33, 49].

However, it is increasingly challenging to simultaneously meet the demand for higher FLOPS and better energy efficiency, due to the *tight coupling* between the matrix units and the GPU SIMT cores. Matrix units are typically integrated into the SIMT core pipeline as specialized functional

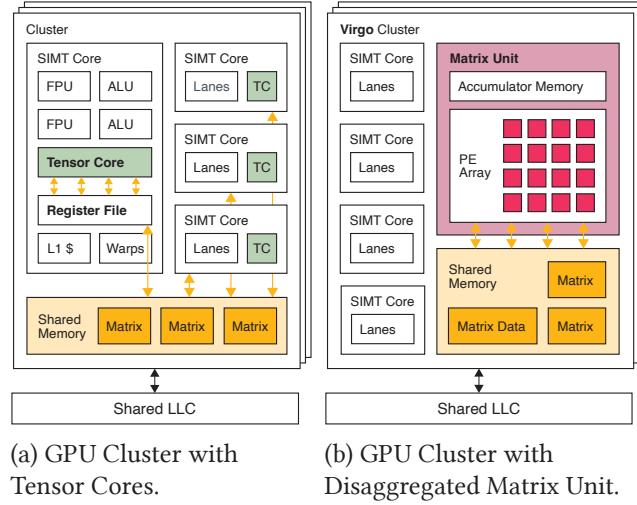


Figure 1. Overview of (a) today’s GPU architecture with tightly coupled integration of Tensor Cores (TC), compared to (b) Virgo’s cluster-level integration of matrix units.

units, receiving data through the register file via the standard instruction datapath. This tightly coupled integration faces significant limitations in terms of operation size due to the capacity and bandwidth constraints of the register file. Consequently, core-coupled matrix units support fine-grained operations, commonly with tile sizes such as 16×8 [35, 39]. Such a small granularity of operation not only limits data reuse, but also requires processing a large number of instructions in the core pipeline, consuming substantial energy and power in instruction scheduling and address generation, rather than in actual computation.

To address these challenges, we propose Virgo, a novel GPU architecture that integrates dedicated matrix units at the *cluster* level (Figure 1). The cornerstone of Virgo is the physical disaggregation of the matrix unit from the core microarchitecture, eliminating scalability constraints and increasing matrix operation granularity. Virgo improves system-level energy efficiency through reducing instruction processing, eliminating redundant register file accesses, and increasing data reuse. Key contributions of our work are:

- We propose a novel cluster-level matrix unit integration methodology for GPUs that enhances scalability and efficiency by disaggregating the accelerator from the SIMT core.
- We fully implement the GPU designs featuring not only the proposed cluster-level integration, but also baseline core-coupled integrations that model Volta, Ampere and Hopper Tensor Cores, in synthesizable RTL. We develop the corresponding software programming interface as well. Virgo is fully open sourced.¹

¹RTL: <https://github.com/ucb-bar/virgo>, kernels: <https://github.com/ucb-bar/virgo-kernels>.

- We demonstrate that Virgo, when synthesized using a commercial 16nm process, significantly reduces active power consumption by 67.3% and 24.2% compared to the Ampere and Hopper-style core-coupled baselines, and energy consumption by 80.3% and 32.5%.

2 Background and Motivation

This section provides an overview of the GPU and Tensor Core microarchitectures, highlighting the scalability and efficiency limitations caused by the tight coupling of the matrix unit to the SIMT core. This discussion motivates Virgo’s key design decision to integrate matrix units at the cluster level, addressing architectural bottlenecks and aligning with the increasing demands of modern GPU applications.

2.1 GPU Cluster Microarchitecture

Figure 1(a) shows the modern GPU microarchitecture, featuring multiple clusters of SIMT cores connected to a shared last-level cache. Each SIMT core consists of a warp scheduler, a register file, and tightly-coupled execution units like Tensor Cores. Within each cluster, SIMT cores are interconnected via a cluster-level network-on-chip to the *shared memory*, a software-managed scratchpad.

The clustered organization offers several benefits. First, it increases hardware parallelism by allowing multiple cores in a cluster to execute independent warp instructions simultaneously. Second, it enables increased data sharing within the kernel, as a greater number of threads across the SIMT cores can share data through the shared memory. This cluster-based architecture is widely adopted in the industry, known as *Streaming Multiprocessors* in NVIDIA GPUs [16], *Compute Units* in AMD CDNA architecture [1] and *X^e-cores* in Intel X^e-HPG architecture [26].

Importantly, the cluster serves as the hardware unit to which a *thread block* or a *workgroup* is assigned, which is a group of SIMT threads that provides software primitives for shared memory access and barrier synchronization [22]. With modern workloads like large language models (LLMs) requiring increasingly large GEMM operations, there is a growing need for improved data reuse at the shared memory level. This necessity motivates the rationale for integrating matrix units at the cluster level, a key principle that guides the development of the Virgo system.

2.2 State-of-the-art Tensor Core Integration

To meet the rapidly increasing compute demand of deep learning applications, NVIDIA introduced dedicated matrix units known as *Tensor Cores* in the Volta architecture [13]. Tensor Core consists of multiple SIMD-parallel dot product units designed for high-throughput multiply-add operations in matrix multiplication [34]. As shown in Figure 1(a), Tensor Cores receive matrix operands directly through the register file of the SIMT core, similar to other execution

GPU	V100	A100	H100
Architecture	Volta	Ampere	Hopper
Tensor FP16 TFLOPS	1x	2.5x	7.9x
CUDA FP32 TFLOPS	1x	1.2x	4.3x
# of Tensor Cores (TC)	1x	0.7x	0.8x
MACs per TC	64	256	512
Register usage (max. 255)	224	221	168
Warp occupancy	12.5%	10.0%	14.1%

Table 1. Scaling trends of the compute capabilities of NVIDIA datacenter GPUs across generations, and occupancy statistics of CUTLASS GEMM kernels on them. The multiply-accumulate (MAC) units per Tensor Core is analytically estimated from FLOPS using the clock frequency. For the kernel statistics, we profile `s884gemm_f16*`, `s16816gemm_f16*` and `sm90*_s64x128x16gemm_f16*` for V100/A100/H100, and compute the average across five kernel parameter combinations with the highest FLOPS for each architecture.

units such as the floating-point unit and the load/store unit. Essentially, today’s Tensor Core is a specialized execution unit for matrix multiplication that is tightly coupled into the execution pipeline of the SIMT core. Prior efforts have focused on improving the Tensor Core design in sparsity support [20, 25, 44] and generalized operations [40, 48], while maintaining the core-coupled integration.

Notably, Tensor Core has been rapidly increasing in its compute capabilities. Table 1 outlines the evolution of NVIDIA datacenter GPUs across generations [13, 14, 16]. The FP16 throughput of Tensor Cores has improved at a rate surpassing that of FP32 throughput in CUDA cores. This increase in throughput is not due to an increase in the number of Tensor Cores, but rather to each Tensor Core instance growing larger in size. This trend underscores the need to scale up the individual capabilities of the matrix units for future generations of GPUs.

2.3 Limitations of the Core-Coupled Approach

However, the tightly core-coupled nature of today’s Tensor Core design poses significant challenges to further scaling of the matrix unit. First, modern GEMM kernels generate high *register pressure* as they require extensive use of register file space to store multiple input and accumulator data [28]. This issue is compounded in kernels that utilize dedicated matrix units, where the entire input and accumulator matrix tiles must be stored within the register file, significantly increasing the register usage. As a result, this leads to decreased kernel occupancy or frequent register spills to stack memory in Tensor Core-accelerated GEMM kernels, as reported in previous studies [7, 41, 43, 45, 47]. Our characterization of CUTLASS GEMM kernels [28] confirms this as well, where high register usage significantly limits warp occupancy of the

kernel (Table 1). Efforts like INTERPRET [30] and Duplo [29] are developed to reduce duplicated data in the register file, alleviating capacity constraints.

Furthermore, the tight coupling to the SIMT core’s register file imposes not only *capacity* constraints, but also *bandwidth* constraints. According to [34], the register read bandwidth available in the Volta architecture is maximally utilized during Tensor Core operations. Scaling up the operation size requires increasing register file bandwidth to deliver larger operand data to the Tensor Core, introducing significant design challenges.

Due to register file constraints, core-coupled matrix unit designs typically support *fine-grained* operations. For example, the NVIDIA Tensor Cores handle tile sizes of $16 \times 8 \times 16$ for FP16 input operands in the MMA instruction [17]; similarly, AMD CDNA2 Matrix Cores supports sizes of 16×16 and $32 \times 32 \times 8$ in the MFMA instruction [35]. These small tile sizes incur additional data transfers from the backing memory due to limited reuse. Additionally, they require processing a large number of instructions and computing extra tile memory addresses to complete the GEMM operation, leading to significant energy and power consumptions in hardware components beyond the matrix unit, including the instruction scheduling logic, ALU, and the register file.

2.4 Recent Advances and Remaining Challenges

Recent industry GPU designs have made advancements in addressing the efficiency and scalability challenges of the core-coupled approach described above. Namely, NVIDIA Ampere Tensor Core introduces Asynchronous Data Copy [15], which adds hardware acceleration for transferring data directly from the global memory to the shared memory, bypassing the core’s register file. By offloading data copy operations from the core, resource usage within the core pipeline—such as register files and instruction slots—is reduced, enabling more efficient allocation of such resources to matrix operations. Additionally, this offloading enables asynchronous overlapping of data movement and compute, improving efficiency compared relying solely on warp concurrency. In our profiling of CUTLASS, we observe 36% less warp stalls in the async-copy-enabled GEMM kernels, which led to 22% increase in issue slot utilization.

Building upon Ampere, NVIDIA’s Hopper Tensor Core, introduced in 2022, further alleviates register pressure with the introduction of the `wgmma` operation. This new mode of operation enables the Tensor Cores to read matrix operands directly from shared memory, reducing dependency on the register file [16, 32]. This new operand delivery method mitigates the need to store the matrix data in the register file, alleviating the scalability limitation. This is evidenced by the significant decrease in register usage that enabled further scale-up of MACs in Hopper, shown in Table 1.

However, the Hopper Tensor Core does not fully solve the register pressure issue, and energy efficiency remains a concern. The wmma instruction, while reducing some register load, still accumulates the partial sum matrices back to the register file [17], generating significant register pressure (Table 1). Furthermore, the Tensor Core still remains physically coupled to the SIMT core [16, 32], preventing data sharing across matrix units that could otherwise be achieved in a large, unified matrix unit design.

Virgo fundamentally address the scalability and energy efficiency challenges by completely disaggregating the matrix unit from the SIMT cores, establishing it as a separate instance at the cluster level. To the best of our knowledge, Virgo is the first effort to integrate a matrix unit at the core cluster. Through disaggregation, Virgo completely bypasses the core's register file for operand and accumulator storage, eliminating its scalability constraints. It also reduces energy consumption in the register file, by offloading data access directly to the shared memory or a separate, energy-efficient accumulator memory. Finally, the disaggregation also enables a unified matrix unit design, which maximizes data reuse across processing elements compared to separate, per-core configuration.

2.5 Terminology and Modeling

To facilitate further discussion, we define a terminology that corresponds to the integration methods described above. This classification allows us to separate different design concerns and facilitate a fair evaluation of our design. Section 5 details how we model each of these design points.

- **Tightly-Coupled Matrix Unit** refers to the traditional design where the matrix unit is integrated within the SIMT core, heavily relying on the register file for both operand and result data delivery. The NVIDIA Volta Tensor Core is an example of this design.
- The Tightly-Coupled Matrix Unit can be extended with a **dedicated DMA**, enabling more efficient data delivery from off-chip to on-chip memory. This configuration corresponds to Ampere, where we assume that Ampere features a separate DMA engine similar to Hopper in order to support Asynchronous Data Copy instructions.
- **Operand-Decoupled Matrix Unit** allows the matrix unit to directly source operand data from the shared memory, but the unit itself remains to be part of the SIMT core. This configuration resembles Hopper.
- **Physically Disaggregated Matrix Unit** refers to Virgo's design, where the matrix unit is completely separated from the SIMT core and externally integrated at the cluster, enhancing data reuse and scalability.

For brevity, we also refer to the above terms as *Volta-style*, *Ampere-style*, *Hopper-style matrix units* and *Virgo*.

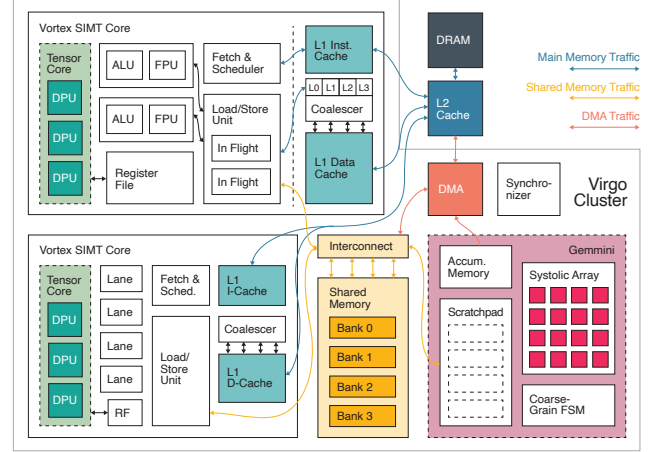


Figure 2. A high level overview of the Virgo microarchitecture. The Gemini-based matrix unit is disaggregated out from the SIMT cores into a separate unit in the cluster. Dashed lines indicate optionally instantiated modules for evaluation, such as the core-coupled Tensor Core.

3 Virgo Microarchitecture

Virgo aims to improve scalability and energy efficiency by disaggregating the dedicated matrix unit from the core as separate hardware at the cluster level, as depicted in Figure 2.

To realize this design, we need to solve several microarchitectural challenges: (1) establishing a command interface through which the core and the unit can communicate, (2) designing a cluster-local shared memory interconnect that efficiently handles concurrent accesses from the core and the matrix unit, (3) facilitating a more efficient matrix data movement via a dedicated DMA engine. and (4) implementing a synchronization mechanism across the cores and the matrix unit. We discuss these components in more detail in the following subsections.

Before we begin, we mention key open-source hardware infrastructures that we leverage to realize our design at the RTL. First, we use Vortex [42], an open-source GPGPU implementation in SystemVerilog that enables the full stack of both hardware and kernel development by extending the RISC-V ISA. Second, we use Gemini [21], a systolic array generator, to generate the cluster-based matrix unit IP for Virgo². We describe in further detail how we modify these IPs to establish a full GPU system in Section 5.

3.1 Command Interface to the Matrix Unit

We facilitate the cluster-local interconnect to establish an efficient memory-mapped IO-based command interface between the core and the matrix unit. The MMIO interface is

²The name *Virgo* is inspired by the use of *Vortex* and *Gemini* to achieve cluster-level integration.

advantageous in our design because it does not require modification of the ISA and the core microarchitecture: At the kernel, the core controls the matrix unit simply by issuing regular loads and stores to a specific memory address region. At the same time, the core still benefits from low-latency access to the memory-mapped registers that are interconnected to the lightweight, cluster-local NoC.

In order to establish the MMIO interface, we replace Gemini's original RoCC interface [6] with memory-mapped control registers that the core can access via the shared memory address space. To synchronize the core threads in relation to Gemini operations, we use a software routine that polls a memory-mapped register that indicates the accelerator's busy state. When performing GEMM, a hardware FSM exists in Gemini to automatically iterate through the i , j and k dimensions, allowing a single invocation to fully compute on matrix sizes larger than the systolic array dimensions. The FSM retrieves operands from the shared memory, controls systolic array operation, and writes the result matrix to the accumulator memory.

3.2 Memory System

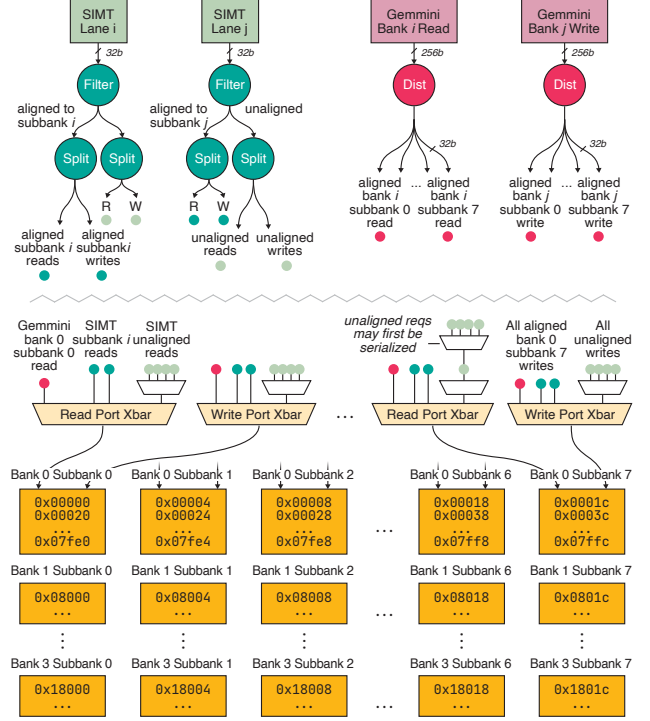
The main challenges of Virgo's memory system involves handling concurrent, heterogeneous accesses to the shared memory from both the core and the matrix unit, and achieving high effective bandwidth in fetching matrix data from the global memory. The following subsections discuss each of these challenges.

3.2.1 Shared memory. The shared memory must efficiently support specific access patterns from both the SIMT cores and the matrix units. Namely:

- The Gemini-based matrix unit generates wide accesses of size $4n$ bytes, where n is the systolic array dimension. On the other hand, the individual lanes of the SIMT core make narrower 4-byte requests.
- The SIMT cores and the matrix unit should be able to concurrently access two different matrices without serialization. This is necessary when they operate in a producer-consumer relationship through double buffering in the memory, as described in Section 4.4.2.

It is also important to keep the hardware complexity of the interconnect manageable while supporting the above access patterns, given that there are many SIMT lanes in the cluster. To tackle these challenges, we make the following key design choices, depicted in Figure 3:

Two-dimensional banking. To accommodate the aforementioned different-sized accesses from the core and matrix units while incurring minimal bank conflicts, we partition shared memory address space in two dimensions: banks and subbanks. This enables parallelism of memory accesses across subbanks, i.e. from SIMT lanes within a core, as well as banks, i.e. from both matrix unit and cores.



accounts for 5.5% of the area and 6.8% of the power consumption in the SoC. Also, compared to a baseline design that does not support Gemmini connection, the shared memory area only increases by 9.6%.

3.2.2 Accumulator Memory. Virgo’s disaggregated matrix unit features a dedicated SRAM memory for storing accumulator matrix data, also shown in Figure 2. Equipping the matrix unit with a dedicated accumulator memory is an important design choice we make for two reasons.

First, this design enables providing the matrix units with a large accumulator data storage without impacting parallelism of the kernel. GPU’s register file space is privatized across different warps in the core, establishing the SIMT abstraction. Because core-coupled matrix units such as Tensor Cores accumulate data and return the result also through the SIMT registers, scaling up the matrix units increases per-warp register usage, and results in higher register pressure and decreased occupancy of the kernel (see also Table 1). While lower occupancy does not always lead to lower matrix FLOPS, it may affect the performance of fused DNN kernels where the activation compute has to run with reduced thread-level parallelism. In contrast, providing matrix units with access to a separate accumulator memory without SIMT privatization decouples the issue of register pressure from the size of matrix compute, and allows the hardware designer to scale up matrix units without worrying its impact to the overall kernel performance.

Second, regular access patterns to the accumulator data enables a simpler and more energy-efficient memory design. Unlike the register file, which must support divergent scatter-gather SIMT accesses, matrix units perform wide and contiguous accesses to the accumulator data. This enables a straightforward SRAM implementation—specifically, the Virgo unit employs a single-banked SRAM, reducing hardware complexity and lowering energy consumption per access. We present quantitative results in Section 6.1.2.

3.2.3 Memory coalescer. *Memory coalescing* [18] plays a crucial role in GPU memory systems by converting scalar SIMT memory accesses into wide, vectorized accesses, and thereby achieving high *effective* memory throughput. At the onset of the project, Vortex had lacked hardware support for memory coalescing, significantly limiting the memory bandwidth of SIMT load and store instructions. To this end, we implemented a custom memory coalescing unit as shown in Figure 2. The coalescer monitors the core’s SIMT memory accesses at the core and L1 cache interface, and opportunistically merges them into wider memory requests of the same size as the L1 cache line. The coalescer significantly increased data delivery rate from the global memory (*i.e.* DRAM, L2 and L1) to the cores, and improved utilization of the matrix units. Note that the coalescer is used for the Tightly-Coupled, Volta-style configuration (Section 2.5), which utilizes SIMT instructions for data delivery instead of a DMA.

3.2.4 Efficient Data Movement with DMA. We further facilitate efficient data delivery to the matrix units beyond what memory coalescing provides by incorporating a dedicated DMA engine. Hardware-accelerated data movement is becoming increasingly common in modern GPU designs. The NVIDIA Ampere architecture introduces Asynchronous Data Copy to accelerate direct memory transfers between global and shared memory [15], while the Hopper architecture features a dedicated TMA engine that supports flexible address generation modes [16]. In our models of Ampere-style and Hopper-style Tensor Core systems, as well as in Virgo, we include a MMIO-programmable DMA engine in the cluster dedicated to issuing direct memory accesses between global memory and shared memory. Additionally in Virgo, the same DMA is capable of drawing from the matrix unit’s accumulator memory as well, depicted in Figure 2.

3.3 Cluster-wide Synchronization

As will be discussed in Section 4, the SIMT cores in a cluster work together collaboratively to either move matrix data to the matrix unit, or do post-processing computation on the resulting matrix from the unit. This requires an efficient synchronization mechanism across the cores to be implemented at the entire cluster level.

To this end, we design a lightweight synchronizer module in the cluster that interfaces with the warp scheduler of each SIMT core. When a designated set of warps reach a barrier instruction in the kernel, the warp scheduler issues a barrier release request to the synchronizer. The synchronizer collects requests from other cores in the cluster, and replies once receiving requests from all cores, ensuring every core participates in the barrier. We reuse Vortex’s `vx_bar` instruction to allow the programmer to specify which warps participate in a particular barrier, and be able to use multiple barriers in the kernel.

4 Virgo Programming Model

As a result of architectural disaggregation from the core, the matrix unit in Virgo operates as a separate thread of execution from the SIMT cores. In this section, we establish a programming model that enables the programmer to efficiently coordinate the matrix unit and the SIMT cores, based on two principles: (1) an asynchronous programming interface and (2) collaborative execution of warps.

4.1 Asynchronous Matrix Unit Interface

Virgo exposes an asynchronous programming interface to allow the programmer to flexibly overlap SIMT core compute concurrently to the matrix operations. As discussed in Section 3.1, the Gemmini-based matrix unit in Virgo exposes a memory-mapped IO interface to the core. The accesses to the MMIO interface are non-blocking, such that a single

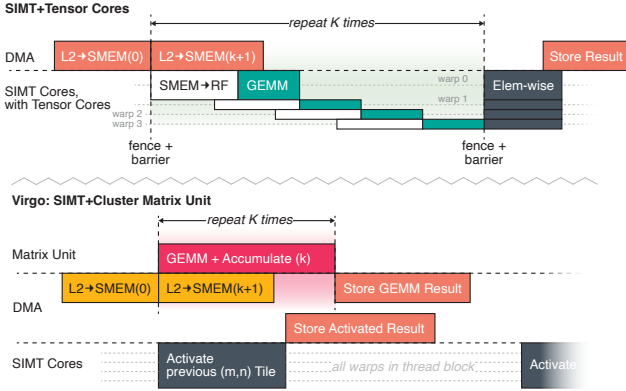


Figure 4. Execution in the SIMT core, matrix unit, and DMA during a GEMM operation on Virgo and Tensor Core-based designs.

SIMT warp can kick off a matrix unit operation and then continue to execute the next instructions in the kernel without stalls. This enables a software-pipelining scheme where the warp can overlap independent operations such as data movement for the next tile or post-processed activation while the long-latency matrix operations occur. We will detail how the programmer can exploit the instruction-level parallelism through this interface in Sections 4.4 and 4.5.

An asynchronous matrix unit design is common in modern GPU architectures. Notably, the NVIDIA Hopper Tensor Core [16] and the AMD CDNA2 Matrix Core [2] support same-warp co-execution of matrix and SIMT vector computations. Without such a mechanism, the SIMT core relies solely on multithreading across multiple warps to hide the latency of matrix operations, which requires high warp occupancy to ensure the scheduler always has unblocked warps for issue. In contrast, the asynchronous interface enables programmers to exploit instruction-level parallelism within a single warp, providing additional opportunities for latency hiding. Virgo particularly benefits from this interface, as its enhanced scalability supports larger tile sizes, which introduce longer compute latencies to be overlapped.

4.2 Collaborative Execution of Warps

GEMM operation on GPUs require close coordination between the core operation and the dedicated matrix unit operation, where the core handles data movement operations between the off-chip and on-chip memory, or post-processing compute on the result matrix such as non-linear activations in a deep learning workload. Therefore, the SIMT cores need to achieve adequate throughput that matches compute throughput of the matrix unit. To this end, in Virgo, *multiple* warps collaborate to participate in a *single* operation of the matrix unit. This is depicted in Figure 4, where all warps in the thread block works on activating the previous (M,N) output tile computed by the matrix unit operation.

The collaborative execution of warps requires the cluster-wide synchronization mechanism described in Section 3.3, because the warps in the thread block may be running in different cores in the cluster.

4.3 API Design

Virgo’s application programming interface consists of two levels: A low-level interface that directly exposes the initiation and synchronization mechanism of the hardware, and a higher-level library that helps the programmer to express GEMM computations. The low-level API is composed of the following operations:

- `virgo_dma_{load,store}` initiates an asynchronous DMA operation to copy the tile across the global memory, the shared memory and the accumulator memory inside the matrix unit. It takes as argument the base addresses of the tiles, matrix dimensions, and their memory layout, which configures the DMA for correct addresses generation.
- `virgo_compute` kicks off the asynchronous matrix multiply-and-accumulate operation in the matrix unit, accessing the tile data from the shared memory.
- `virgo_fence` blocks the warp until all preceding asynchronous operations have completed and their results are visible to the programmer.

As described in the previous section, these API calls are used in conjunction with the cluster-wide synchronization barrier to ensure all participating cores remain synchronized in relation to the matrix operation.

On top of the low-level API, we provide a library that constructs a full GEMM kernel using tiled matrix multiplication. The library consists of C++ templates that, given GEMM dimension constants, instantiates to a concrete kernel specialized to each GEMM size by determining (M,N,K) loop iterations at compile time. Using the library, the programmer can easily invoke a device-level GEMM kernel without worrying about the details of mapping to the matrix unit, or write a fused kernel that includes a GEMM component.

This API design is similar to existing GPU GEMM libraries such as Composable Kernel [3] or CUTLASS [28], which similarly construct a hierarchy of API layers on top of the hardware-dependent, tile-level operators. One difference is that, in Virgo, the indivisible *atom* of computation is a threadblock- or workgroup-level matrix multiplication as a result of the enlarged tile size, while the other libraries map to finer-grained operations at the warp or warpgroup-level atoms. Virgo’s larger compute unit enables more optimal hardware scheduling decisions while reducing instruction processing overhead within the core, as discussed in as discussed in Section 6.1.2. However, this approach sacrifices flexibility for workloads that use smaller matrix dimensions.

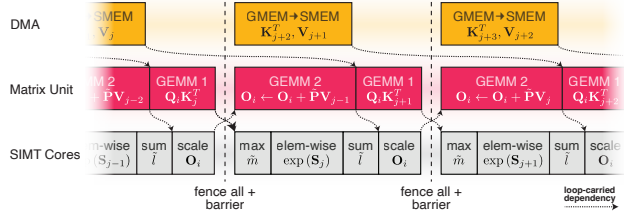


Figure 5. FlashAttention-3 mapping to Virgo.

4.4 Mapping to the GEMM Kernel

We now describe how the aforementioned programming model can be used to write an optimized GEMM kernel.

4.4.1 Thread block tiling. We extend the well-established work partitioning scheme of GEMM kernels on GPUs, which employs tiling of the input matrices at *multiple* levels to maximize data reuse at the different memory hierarchy [28]. Virgo’s matrix unit accelerates the first level of *thread block* tiling, which leverages parallelism across clusters and caches tiles at the shared memory. In comparison, Tensor Cores accelerate the second level of *warp* tiling.

In our configuration, the matrix unit exposes $128 \times 64 \times 128$ as the tile size of a single operation, which determines the thread block size. Each thread block, spatially partitioned across the (M,N) output space, completes the full GEMM by accumulating across the K dimension temporally in a loop, shown in Figure 4. As the loop iterates, the Gemini matrix unit accumulates partial sum data onto its private accumulator memory, which gets moved out and stored to the global memory at the end of the loop. Then, the kernel moves on to the next (M,N) output tile that is allocated to that thread block. The kernel can launch multiple thread blocks, where the (M,N) output space is divided equally across the thread blocks.

4.4.2 Software pipelining and double buffering. Importantly, the Virgo-optimized GEMM kernel employs *software pipelining* which is enabled by the asynchronous programming interface of the matrix unit. As shown in Figure 4, while the matrix unit is computing a tile along the K dimension consisting a *consumer* pipeline, either the DMA unit or a set of SIMT core warps collaboratively fetch the next input tile along the K dimension from the global memory to the shared memory, consisting the *producer* pipeline. Another set of SIMT core warps can collaborate to form an additional consumer pipe that does post-processing activation compute on a previous result tile. Because both the producer and consumer pipes run in parallel, the tile data are double-buffered in the shared memory. This mechanism allows both the SIMT core warps and the matrix unit to participate in useful work at all times, maximizing utilization of all hardware components in the cluster.

4.5 Mapping to FlashAttention-3

To better illustrate the flexibility of Virgo’s programming model, we demonstrate how to map FlashAttention-3 [37], a GPU kernel that fuses the self-attention layer in the Transformer architecture, to Virgo. Detailed utilization and energy measurements for this kernel are provided in Section 6.2.

FlashAttention-3 defines three compute pipelines that can be overlapped to improve hardware utilization: (1) *GEMM-1* of Q and K^T tiles, (2) *GEMM-2* of P and V tiles, and (3) softmax. In the Virgo microarchitecture, we can map the two GEMMs sequentially to the matrix unit, and the softmax to the SIMT core, allowing both to execute concurrently. Given the producer-consumer relationship between the GEMM and softmax pipelines, we use fence calls and cluster-wide barriers to synchronize and enforce ordering across compute units. This enables a software-pipelined mapping onto the hardware, along with double-buffering of intermediate tiles in shared memory. Figure 5 illustrates this mapping scheme. Listing 1 provides simplified pseudocode of a Virgo kernel implementing this scheme. In the loop iterating over tiles, the SIMT threads initiate matrix unit operations for the two GEMMs, and DMA operations to preload tile data into shared memory for the next iteration. Since all operations are asynchronous, threads can immediately proceed with the softmax computation within the SIMT core. Notably, because both the GEMM and softmax pipelines access the same activation tile (smem_0), an additional fence is required. This fence only blocks until the GEMM-2 operation completes, without affecting subsequent operations.

```
for (int iter = 0; iter < tiles; iter++) {
    // block until all previous-iter async ops complete
    virgo_fence(0);
    // synchronize cores cluster-wide at every loop iteration
    threadblock_barrier();
    // double-buffer SMEM tile addresses
    smem_Pp = (iter%2) ? smem_P0 : smem_P1; // produce
    smem_Pc = (iter%2) ? smem_P1 : smem_P0; // consume
    ...
    // initiate asynchronous matrix ops
    // GEMM-2: O = O + P*V
    virgo_compute(smem_Pc, smem_Vc, smem_O, /*accum=*/1);
    // GEMM-1: S = Q*K
    virgo_compute(smem_Qc, smem_Kc, smem_Sp, /*accum=*/0);
    // asynchronously copy K and V tile for the next iter
    virgo_dma_load(gmem_K, gmem_V, smem_Kp, smem_Vp, ...);
    ...
    // overlap with SIMT softmax compute
    online_softmax(smem_Sc, smem_Pp, per_row_scale, ...);
    // block until the 2 most recent operations (GEMM-2)
    virgo_fence(2);
    row_rescale(smem_O, per_row_scale);
}
...
// copy final activation tile to global memory
virgo_fence(0);
virgo_dma_store(gmem_O, smem_O);
```

Listing 1. Pseudocode of FlashAttention-3 on Virgo.

4.5.1 Synchronization Overhead. To maximize overlap and achieve high utilization in the mapping scheme described, the synchronization between the core and the matrix unit must have minimal overhead. To assess this, we measure the cycle times the core spends in the busy register polling loop within the `virgo_fence` operation. On average, this interval is 260 cycles, which accounts for 2.4% of the total runtime. This indicates that the kernel exploits high instruction-level parallelism, as all remaining cycles overlap matrix operations with SIMT computations.

The synchronization overhead also depends on the pipelining scheme used for the workload and its throughput-matching behavior. In our experiment, the softmax execution completes slightly earlier than the GEMM. In workloads where pipeline throughputs are ideally matched, or where the matrix computation completes first, the synchronization overhead can be lower than what we measure.

5 Methodology

In this section, we outline how we implement both our proposed microarchitecture and the baseline GPU designs in RTL, and then set up experiments for evaluation.

5.1 Baseline GPU Designs

We first describe how we implement the baseline GPU designs that feature core-coupled integration methods of matrix unit. We continue to follow the classification we established in Section 2.5, and focus on how to faithfully model each of the design points. This allows us to better evaluate our design in a way that achieves separation of concerns without conflating multiple design considerations at play.

5.1.1 Volta-style Tightly-coupled Design. The Volta-style design features matrix units tightly coupled to the core’s register file. For its implementation, we closely refer to the microarchitecture proposed in [34], whose timing behavior is correlated with the NVIDIA GPU. The microarchitecture features SIMD-parallel dot-product units, composed of floating-point units in a tree-reduction configuration, that execute multiply-and-accumulate (MAC) operations on the input tile fragments. As a result of tight coupling, the tile fragments are directly supplied from the register file via core pipeline, and the result fragments are written back to the register file as well.

We extend the Vortex RISC-V ISA to control the matrix unit, modeling Volta’s HMMA SASS instructions. Specifically, a single tile operation is split into finer-grained *set* and *step* instructions, sequenced to perform the inner and outer products of the input tile fragments. It is worth noting that the Ampere and Hopper Tensor Cores manage the sequencing of sets and steps at the microarchitecture level [34, 39], reducing the overall instruction count. We model this mechanism in the Hopper-style baseline as well.

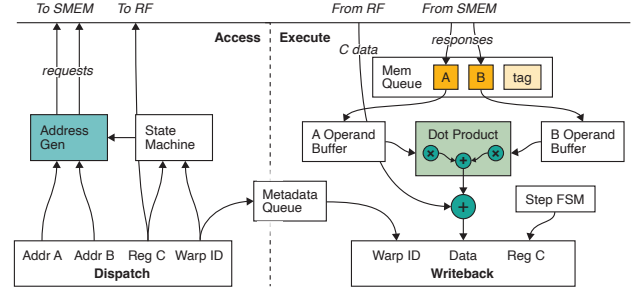


Figure 6. Microarchitecture of the decoupled Tensor Core, which models NVIDIA Hopper’s integration scheme of decoupling operand storage to the shared memory [10]. The decoupled access/execute architecture effectively overlaps the access latency to the shared memory with compute.

Since our Vortex core configuration has a narrower SIMT width than Volta (8 vs. 32), we correspondingly scale the design to achieve full efficiency of the hardware. Specifically, we instantiate a single octet instance instead of four in the original design [34]. The tile size of a single wmma instruction is determined by the register file space. As discussed in Section 3.2.2, Tensor Core operates at a per-warp granularity, and therefore can access the register space SIMT-privatized to each warp, which is 1 KiB in our configuration. This space allows storing two 8×16 FP16 operands and one 8×8 FP32 accumulator tile, resulting in the tile size of $(m, n, k) = (8, 8, 16)$. The available read bandwidth from the register file limits the number of FP16 MACs per unit to 32. Our resulting Tensor Core implementation maintains the same timing behavior of 2 cycles per HMMA *step* instruction as in Volta, along with an identical Tensor-to-SIMT FLOPS ratio of 4:1.

5.1.2 Ampere-style Tightly-coupled Design with DMA.

The Ampere-style baseline features tightly-coupled matrix units and a dedicated DMA incorporated into the GPU. To model this baseline, we use an identical matrix unit module as the Volta-style baseline, but additionally instantiate a DMA unit described in Section 3.2.4.

Note that publicly available information does not explicitly confirm whether the Ampere architecture includes a dedicated DMA engine similar to Hopper [15]. However, to more clearly isolate the impact of different design components in our evaluation, we introduce DMA in the Ampere-style design and incrementally incorporate operand decoupling in the Hopper-style design.

5.1.3 Hopper-style Operand-decoupled Design.

The Hopper-style baseline enhances the matrix unit design by enabling direct access to operand matrix data from shared memory, while accumulator data continues to be both read from and written to the register file [17]. To implement this

design, we extend the Volta-style matrix unit implementation into a decoupled access-and-execute architecture [38], illustrated in Figure 6. The *access* frontend includes a state machine and an address generation module that issues a sequence of read requests to the matrix fragments stored in the shared memory. The *execute* backend comprises decoupling FIFO queues and operand buffers, which stage the responses from shared memory and perform MAC operations when operand data becomes available. Since the addresses of the matrix fragments are statically determined, the access frontend can run ahead of the execute backend, effectively hiding shared memory access latency.

We expose an asynchronous instruction interface for the Hopper-style through ISA extension that models the wmma PTX instruction [17]. A warp kicks off the matrix unit via an *initiate* instruction without stalling, and later executes a *wait* instruction to synchronize with the unit and retrieve a valid result. Similar to Virgo, this asynchronous design enables instruction-level parallelism within a single warp.

While offloading operand data alleviates capacity constraints, storing accumulator data in the register file continues to limit tile size. Similar to Volta, the Hopper unit has access to 1 KiB of register space per warp, accommodating up to a single 16×16 FP32 accumulator tile. There is no significant constraint to the shared-memory-stored operand tile size; however, a large k tile dimension is not necessarily advantageous as there is no data reuse over k . Consequently, the maximum tile size we support in the Hopper unit is $(m, n, k) = (16, 16, 32)$. The number of MACs in the unit is constrained by the shared memory bandwidth, which is 64 FP16 operations per cycle in our configuration. This achieves the Tensor-to-SIMT FLOPS ratio of 8:1.

Note that the Hopper-style design also incorporates a dedicated DMA, similar to Ampere-style and Virgo.

5.2 System Implementation

We leverage and extensively modify several key pieces of open-source hardware infrastructure to enable our full system at the RTL level. At the top, we use the Chipyard SoC generator framework [4] to integrate all hardware components into a single SoC design: Vortex SIMT cores, matrix units, shared memory, cache, interconnects, etc. Parameters such as the number of cores and clusters, the size and data type of the matrix unit, as well as memory bus widths can all be adjusted, allowing Virgo to be a flexible and comprehensive generator covering a large design space.

Vortex SIMT Cores. We take the SIMT core module from Vortex [42] (vx_core) to construct our own cluster hierarchy and synchronization mechanisms, rather than incorporating the full top-level design. We also adapt Vortex’s cache bank for our L1 cache, positioned after the coalescer.

We made changes to the core pipeline to facilitate higher instruction and memory throughput. These include store

GPU SoC Configuration	
Clusters	1
Cores per cluster	8 in Volta-style / 4 in Hopper-style
SIMT Width	8 warps/core, 8 lanes/warp
SIMD Units	2 ALUs, 1 FPU, 32 LSQ entries per lane
Register File	8KB INT, 8KB FP per core
Shared Memory	128 KB, 4 banks, 8-16 sub-banks
Cache	16KB L1I, 16KB L1D per core, 512KB L2
Volta and Ampere-style Tightly-coupled Matrix Unit	
# of Units	1 per core, 8 per cluster
MACs (Tensor:SIMT)	32 FP16 (4:1) / 16 FP32 (2:1)
Hopper-style Operand-decoupled Matrix Unit	
# of Units	1 per core, 4 per cluster
MACs (Tensor:SIMT)	64 FP16 (8:1) / 32 FP32 (4:1)
Virgo Disaggregated Matrix Unit	
# of Units	1 per cluster
Systolic Array	16×16 FP16 / 8×8 FP32
Accumulator Memory	32KB

Table 2. Hardware configuration of the GPU designs used for evaluation.

fencing, optimized warp scheduling, synchronization, among others. Finally, we added Tensor Cores to the pipeline.

Gemmini-based Matrix Unit. We make extensive modifications to Gemmini [21] in order to make the systolic array directly interface with the cluster-level shared memory. Gemmini coordinates the movement of the source matrices from its private wide scratchpad banks through its systolic array, accumulating at either the individual processing elements or at its private accumulator memory, depending on the selected dataflow. For Virgo, we retained the accumulator memory to ensure full systolic array throughput, which required single-cycle accumulation. We modified the scratchpad interface to use the TileLink protocol and go through the SMEM interconnect, instead of directly interfacing with SRAMs. The SIMT cores can therefore deposit data into the SMEM directly for Gemmini to process.

5.3 Experiments

In this subsection, we will detail the environment in which the workloads are run, the specifics of the kernels, as well as the tools we use to run them.

Hardware Setup. We summarize in Table 2 the hardware configuration of the GPU designs we evaluate, with the GPU SoC configuration being shared by all. Both the Tensor Core and Virgo matrix unit uses fully-pipelined 1 op/cycle *hardfloat* [23] units to implement floating point MACs. All configurations possess the same number of MACs per cluster for a fair comparison.

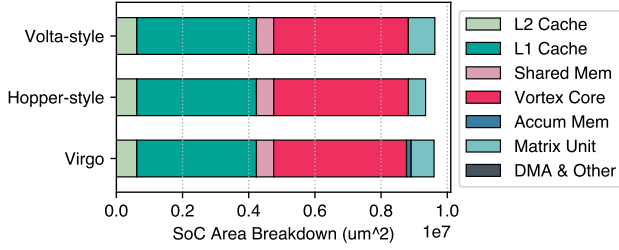


Figure 7. SoC area breakdown of the evaluated GPU designs.

Workloads. We implement GEMM kernels independently optimized for Virgo and baseline designs, with different sizes: $256 \times 256 \times 256$, $512 \times 512 \times 512$, and $1024 \times 1024 \times 1024$, all of which are stored in FP16. We write the kernels in C++ and use Vortex’s LLVM compiler toolchain to generate binaries.

To demonstrate how the SIMT cores can effectively collaborate with the cluster-level matrix unit in a realistic workload, we implement the aforementioned FlashAttention-3 [37] onto FP32 configurations of Virgo and Ampere-style baseline designs. We evaluate the forward pass with a sequence length of 1024, head dimension of 64 with a single head, and a batch size of 1. As the Vortex core lacks a multi-function unit that accelerates exponential operations, we use a 2nd-order Taylor approximation for exponentials, an optimization found in other literature as well [5, 46].

Tools & Measurement. We synthesize the design at 400 MHz using a commercial 16 nanometer process. We use Cadence Joules to estimate power, and use Cadence Genus to estimate area, as well as to verify the operating frequency. An area breakdown of the synthesized SoC design configured to Table 2 is shown in Figure 7. The Virgo design achieves 0.1% smaller SoC area than the Volta-style design, and 3.0% larger area than the Hopper-style design. The L1 cache consumes a large area as it is synthesized as flop arrays rather than SRAMs; however, this did not affect the key findings in our evaluation. Additionally, we used FireSim [27] to verify the design to be functional on a Xilinx Alveo U250 FPGA.

For all power and energy evaluation in the subsequent sections, we plot and discuss *active power*. This metric is obtained by taking the nominal SoC package-wide power, and subtracting the power usage when it’s fully idle. This is necessary to provide a fair comparison, as the baseline idle power is highly implementation-dependent. For instance, we find the power consumption of the Vortex core to be very high at idle when synthesized as ASIC; this is potentially because the core design targets the FPGA environment, with common use of flop arrays and lack of clock gating. By measuring the active power over idle, we can accurately characterize the power implications of our design distinctly from the incidental inefficiencies in the core implementation.

	MAC % Utilization		
	256×256×256	512×512×512	1K×1K×1K
Volta-style	25.6	30.3	30.3
Ampere-style	37.5	45.6	52.3
Hopper-style	60.5	72.8	77.0
Virgo	66.1	77.9	86.5

Table 3. MAC unit % utilization of the GEMM kernel, compared across the GPU designs with tightly-coupled matrix units (*Volta-style*), tightly-coupled matrix units with DMA (*Ampere-style*), operand-decoupled matrix units (*Hopper-style*), and Virgo.

6 Evaluation

We now discuss how Virgo’s disaggregated integration leads to power and energy reduction and utilization improvement using quantitative measurements from RTL simulation and synthesis. We focus on two metrics: power/energy consumption and MAC hardware utilization, across two workloads: GEMM and FlashAttention-3 [37].

6.1 GEMM Kernels

We first evaluate the GEMM kernels on both the cluster-integrated Virgo design and the three baseline core-coupled designs, as described in Section 5.1. Virgo achieves higher MAC utilization across all GEMM configurations. Virgo is also up to 67.3% more power efficient and 80.3% energy efficient than the Ampere-style core-coupled design, as well as 24.2% more power efficient and 32.5% more energy efficient compared to the Hopper-style operand-decoupled design. We elaborate on the performance, power and energy advantage below.

6.1.1 GEMM Performance. Table 3 lists the cycle count and utilization figures for the three GEMM sizes. As shown in the table, the cluster-level matrix unit in Virgo achieves improved MAC utilization compared against all three baselines described earlier.

Virgo achieves higher utilization mainly by enlarging the granularity of operation, and thereby reducing the number of additional instructions that need to be executed in the core pipeline. The Volta-style tightly-coupled Tensor Core is driven by fine-grained instructions with a smaller tile size of 8×8 , which means the SIMT cores need to execute more Tensor Core instructions to complete the full GEMM. Moreover, the input matrix elements need to be loaded into the register file via load instructions from the shared memory, each of which is also preceded by additional address generation instructions. This overall increased number of instructions leads the matrix unit utilization to become constrained by the instruction throughput available from the SIMT core. We

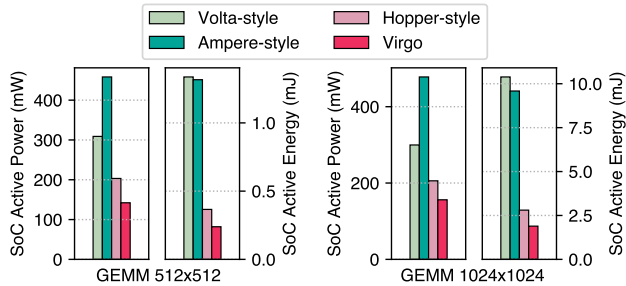


Figure 8. Active power and energy comparison between Virgo and the three baseline core-coupled designs.

note that such constraint can be partially alleviated by microarchitecture improvements in the core, such as dual-issue of instructions.

In contrast to Volta and Ampere, the Hopper-style operand-decoupled Tensor Core significantly reduces instruction overhead within the core through three key factors. First, by increasing the tile size to $16 \times 16 \times 32$ (Section 5.1.3), it lowers the number of matrix operations issued for a given GEMM dimension. Second, unlike the fine-grained, synchronous Volta-style instructions, the unit is driven by a microarchitectural state machine [34, 39], further reducing kernel instructions. Third, similar to Virgo, it autonomously retrieves operand data from shared memory, eliminating load instructions in the kernel. Consequently, the Hopper unit achieves significantly higher utilization than the tightly-coupled baselines.

In a similar manner, Virgo further increases the tile size to $128 \times 64 \times 128$, minimizing MAC utilization constraints imposed by the core’s available instruction throughput.

Instruction statistics support this observation: the number of retired instructions in Virgo is only 0.5% of those in the Volta-style Tensor Core design and 8.0% of those in the Hopper-style operand-decoupled Tensor Core design.

6.1.2 GEMM Power & Energy. In Figure 8 we show a side-by-side comparison between the power usage of Virgo and the three Tensor Core baselines running two GEMM sizes. Virgo enables a 67.3% and 24.2% reduction in active power compared to the Ampere and Hopper-style baselines, respectively. The overall higher power consumption of the Ampere-style design over Volta-style may initially seem unintuitive, but is explained by the higher hardware utilization, enabled by DMA via better operand delivery.

To better reason about the source of power consumption in the hardware, we give a detailed power breakdown at the SoC (Figure 9), the SIMT core (Figure 10), and energy breakdown at the matrix units (Figure 11). At the SoC level, the Vortex SIMT core is a major component in the overall power consumption. Importantly, comparing Virgo to the Tensor Core designs reveals that most power reduction

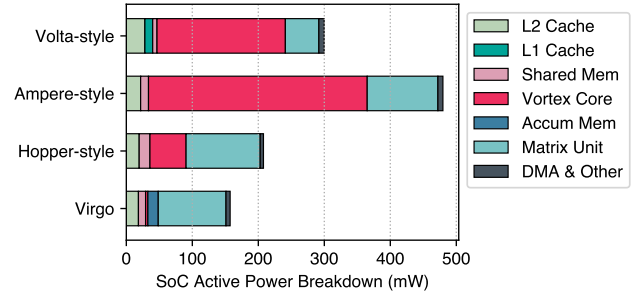


Figure 9. Active power breakdown by SoC components running 1024×1024 GEMM. The core active power is reduced significantly as a result of reduced instruction processing and register file accesses in Virgo.

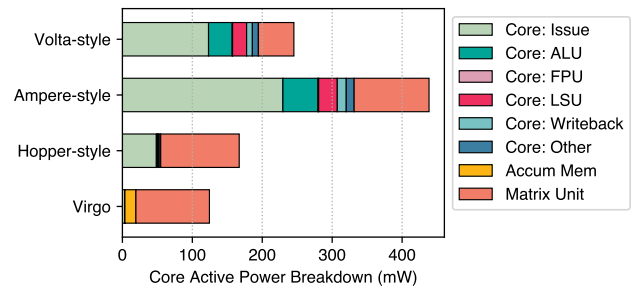


Figure 10. Active power breakdown within the Vortex SIMT core running 1024×1024 GEMM. The Virgo matrix unit component is included for comparison, although it resides outside of the SIMT core.

occurs within the core rather than in the matrix units themselves. We now outline the key factors contributing to such power savings.

Larger operation granularity and reduced instructions. Figure 10 highlights a major difference in core power consumption, particularly in the issue and ALU stages, when comparing Virgo and Hopper-style designs to Volta/Ampere-style designs. This significant power reduction is primarily attributed to the substantial decrease in the number of kernel instructions, as explained in Section 6.1.1. Executing fewer instructions in the core reduces energy consumption associated with dynamically dispatching the instructions via the scoreboard and the warp scheduler, which is reflected in the issue stage power. Additionally, the larger tile sizes in Virgo and Hopper decrease the number of address generation instructions required for the base memory address of each tile, contributing to lower ALU energy consumption. Collectively, Virgo’s larger operation granularity minimizes incidental power consumption in the hardware logic outside the matrix unit.

Offloading operand access from the register file. Beyond instruction processing, accessing the register file for

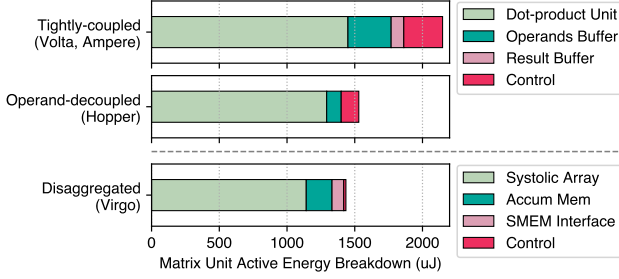


Figure 11. Active energy breakdown of the matrix unit for the 1024×1024 GEMM kernel.

operand delivery also significantly impacts core power. In a Volta-style tightly-coupled Tensor Core, operand matrices are accessed by fetching register operands from the register file as encoded in the instruction. Staging the operands through the register file incurs additional energy compared to accessing them directly from the shared memory, as both the Hopper-style and Virgo matrix units do. This design choice explains the significant reduction in the issue stage power, which includes register file access power, from the Ampere-style to Hopper and Virgo figures.

Decoupled accumulation. Although the operands are offloaded, the Hopper-style operand-decoupled Tensor Core continues to access accumulator data from the core register file. This explains the nontrivial core issue stage power consumption in the Hopper-style baseline (Figure 10). In contrast, Virgo takes an additional step by offloading accumulator data from the register file to a dedicated SRAM-based accumulator memory. The accumulator memory is single-banked, unlike the multi-banked register file that needs to support divergent SIMT accesses, reducing energy consumption per access. In addition, the Virgo matrix unit’s systolic array architecture allows accumulation to partially occur within the mesh, reducing the number of accesses to the memory and further saving power.

Energy consumption in matrix units. Figure 11 shows the active energy consumption of the matrix unit in isolation. We focus on energy rather than power for the matrix unit, because energy directly correlates with the total FLOPs which is kept the same across the designs. The figure does indicate that energy consumption in the matrix unit, especially within the processing elements (“Dot-product Unit” and “Systolic Array”), is similar across the designs. The PE energy is slightly lower for Virgo, due to its use of fused multiply-add units in the systolic array, which are more energy-efficient than the separate multipliers and adders used in Tensor Core’s tree-reduction PEs [34]. However, this difference in the matrix unit energy is minuscule compared to the overall system-level energy savings at the SoC (Figure 8). This suggests that Virgo’s advantages in power and

	Tile Fragment	Matrix Unit Design	SMEM Footprint	
			MiB	Norm.
Tightly-coupled	8×8	Per-core	6	2.67
Operand-decoupled	16×16	Per-core	4	1.78
Disaggregated	16×16	Per-cluster	2.25	1.00

Table 4. On-chip shared memory read footprint compared across the GPU designs. Virgo’s disaggregated matrix unit improves data reuse by (1) enlarging tile size over the tightly-coupled design, and (2) unifying into a single cluster-level unit over the operand-decoupled design.

energy efficiency primarily come from the aspects of operation granularity and operand/accumulator offloading, rather than from choosing a specific design for the matrix unit.

6.1.3 Data Reuse in the Shared Memory. Table 4 lists the shared memory read footprint for the 256×256×256 GEMM kernel. “Tile fragment” refers to the amount of matrix data transferred from shared memory to compute units in a single access. Its size depends on the backing memory internal to the matrix unit that stages data between shared memory and PEs: the operand buffer for both tightly-coupled and operand-decoupled Tensor Cores, and the systolic array registers for Virgo. Unlike the tightly-coupled design, where tile size is severely constrained by the register file space, operand-decoupled and disaggregated designs increase tile fragment size by offloading operand storage, improving data reuse as seen in the lower footprint.

More importantly, Virgo further improves data reuse beyond the operand-decoupled design by unifying the matrix units into a single instance at the cluster level. This unified design enables data sharing in scenarios where non-unified Tensor Cores would otherwise duplicate shared memory accesses. Specifically, in GEMM, different Tensor Cores may compute output tiles along the same row or column. However, due to their physical separation across cores, they must independently access the input row or column data multiple times. In contrast, a unified design allows complete reuse of input matrix data, which explains the further memory footprint reduction for Virgo compared to the Hopper-style operand-decoupled design.

This reduction in memory footprint has both performance and energy implications. We had to scale up the shared memory bandwidth by 2x for Volta and Ampere-style designs with a more aggressive banking strategy, because otherwise the matrix unit utilization would be bottlenecked by memory bandwidth. In one configuration, this change increased utilization from 46.9% to 55.0%. With better data reuse, Virgo achieved optimal utilization without demanding higher memory bandwidth. Energy-wise, the shared memory in the Virgo design consumed 41.0% less active energy compared to the operand-decoupled design.

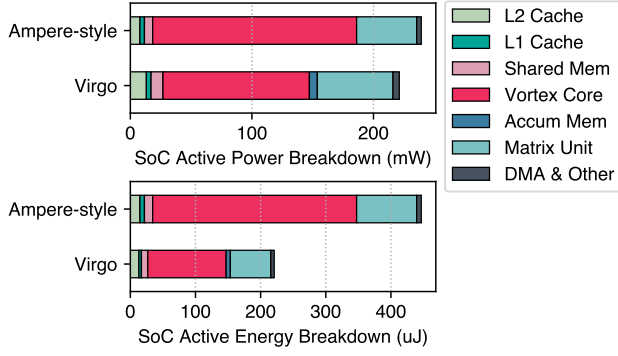


Figure 12. FlashAttention-3 active power and energy breakdown.

6.2 FlashAttention-3 Kernel

We perform a similar analysis of performance, power and energy for the FlashAttention-3 kernel [37], whose mapping to Virgo is described in Sections 4.5 and 5.3. We compare Virgo against the Ampere-style design with tightly-coupled matrix units and an integrated DMA. For the Ampere-style design, the kernel mapping adopts the warp specialization and ping-pong scheduling approach detailed in [37], where the 8 warps within a core are divided into two groups of 4, with GEMM and softmax computations scheduled alternately across the two warp groups. Although the Ampere-style matrix unit lacks single-warp asynchronous execution, it can still co-execute alongside SIMT vector units across different warps, provided the warp scheduler can find eligible warps to concurrently multi-thread.

Performance & Utilization. We observe a total MAC utilization of 65.7% for Virgo, a significant increase over 35.1% for the Ampere-style baseline. The higher utilization is explained by the disaggregated design enabling more efficient allocation of core pipeline resources to non-matrix computations. Since matrix computations are offloaded to a disaggregated hardware, a single warp, after asynchronously initiating the GEMM operation, can reallocate all of its pipeline resources such as instruction slots and register file space to softmax computation. In contrast, the tightly-coupled matrix unit operates through synchronous, fine-grained instructions, meaning that both matrix and softmax instructions need to compete for instruction issue slots and limited register file ports at every cycle. This leads to suboptimal parallelism compared to the disaggregated design.

Power & Energy. We plot the active SoC-level power and energy consumptions of the two designs in Figure 12. As a result of fusing matrix operations with SIMT operations, the core power constitutes more than 50% of the total power for both designs. However, due to the larger operation granularity and offloading of data delivery from the register

file as discussed in Section 6.1.2, the core power consumption is reduced for Virgo, substituted with the matrix unit power operating at a higher utilization. Compounded with the shorter overall runtime of the kernel, the overall energy consumption of the kernel is reduced by 50.6% compared to the Ampere-style baseline.

6.3 Multiple Heterogeneous Matrix Units

The disaggregation of matrix units and parameterized memory system of Virgo allows scaling to multiple matrix units within a cluster. We showcase a configuration where we integrate two differently sized matrix units in one cluster, and map two differently sized GEMMs on them: a $256 \times 256 \times 256$ GEMM onto the large unit, and a $128 \times 128 \times 128$ GEMM onto the small unit. When the two GEMMs run in parallel, we achieve a utilization of 59.5%, compared to 59.7% when they are run separately in serial. The active power when normalized by FLOP increased by only 4.3% for the parallel case. The minimal performance degradation and power overhead demonstrates the scalability of Virgo’s design.

7 Conclusion

We introduce Virgo, a novel GPU architecture that integrates matrix units at the cluster level. By physically disaggregating the matrix unit from the core pipeline, Virgo overcomes scalability and energy efficiency limitations in the current core-coupled GPU designs. This approach enables a heterogeneous GPU architecture optimized for DNN workloads, where SIMT cores and matrix hardware are decoupled for improved scalability while also supporting concurrent execution through efficient command and memory coordination.

We implement and evaluate our design using synthesizable RTL, which shows significant power and energy efficiency improvement for GEMM operations. Furthermore, the decoupled architecture in conjunction with our programming model enables efficient mapping to fused DNN kernels, enabling new strategies for applications mapping.

Acknowledgments

We would like to thank our shepherd Joseph L. Greathouse, the anonymous reviewers and artifact evaluators for their valuable feedback. We would also like to thank Amir Gholami for providing access to a server with NVIDIA GPUs that we used to characterize GEMM kernels. Lastly, we extend our sincere thanks to Kostadin Ilov for his management of the compute servers we used for development.

This research was partially funded by NSF Awards 2303735 and 2238346, as well as by SLICE Lab industrial sponsors and affiliates. The views and conclusions contained in this document are those of the authors and should not be interpreted as representing the official policies, either expressed or implied, of the U.S. Government.

A Artifact Appendix

A.1 Abstract

We evaluate the artifacts of this paper via RTL simulation of the implementation of our proposed GPU microarchitecture, executing two main workloads: GEMM and FlashAttention-3 kernels. We use cycle numbers from the RTL simulation to evaluate hardware utilization, energy measurements, and memory footprint metrics discussed in the paper.

A.2 Artifact check-list (meta-information)

- **Compilation:** GPU kernel compiled with Vortex LLVM compiler, RTL elaborated using Chisel and Chipyard.
- **Hardware:** Ubuntu 20.04 server with Synopsys VCS installed.
- **Metrics:** Cycle time from the RTL simulation, power and energy consumption, MAC hardware utilization, memory footprint.
- **Output:** Microarchitectural trace log, cycle reports in CSV, utilization numbers, plots in PDF.
- **Experiments:** RTL simulation of GPU hardware executing GEMM and FlashAttention-3 kernels.
- **How much disk space required (approximately)?:** 150GB
- **How much time is needed to prepare workflow (approximately)?:** 30 mins
- **How much time is needed to complete experiments (approximately)?:** 30 hours
- **Publicly available?:** Yes
- **Code licenses (if publicly available)?:** BSD-3, Apache
- **Archived (provide DOI)?:** Planned

A.3 Description

As discussed in Section A.6.5, our RTL implementation requires the Synopsys VCS compiler for correct and reproducible simulation. The following setup instructions need to be carried out on a Linux compute server that has access to a working VCS installation. Aside from VCS, all code and peripheral data will be set up from scratch.

A.4 Installation

A.4.1 How to access. Obtain the artifact tarball from <https://doi.org/10.5281/zenodo.14835068>. The artifact consists of:

- Chisel RTL implementation of the Virgo design,
- GPU kernels evaluated on the Virgo implementation,
- Chipyard framework [4] that integrates IPs into an SoC,
- Post-processing and plot generation scripts, and
- Prebuilt Vortex [42] toolchain binaries.

Please note that we provide up-to-date source code and instructions at the public Github repositories <https://github.com/ucb-bar/virgo> and <https://github.com/ucb-bar/virgo-kernels>.

A.4.2 Extracting tarball. In a Linux shell, run the following commands:

```
curl -O "https://zenodo.org/records/14835069/files/virgo-artifact-full.tar.gz?download=1"
tar xzvf virgo-artifact-full.tar.gz
cd virgo-artifact-full/
```

We will refer to `virgo-artifact-full/` as the *root directory* going forward.

A.4.3 Setting up Chipyard. At the root directory, run the following:

```
cd chipyard
# this might take ~10 minutes
./build-setup.sh riscv-tools --skip-submodules
↪ \
--skip-firesim --skip-marshall
```

A.4.4 Compiling Virgo kernels. At the root directory:

```
cd virgo-kernels

Inside virgo-kernels, lib contains the Vortex SIMT core runtime and its header files. kernels contains the source code for the kernels. Run the following to compile all kernels:

source ./scripts/toolchain_env.sh
# compile the Vortex runtime static library
make -C lib
# compile GEMM kernels for Virgo
cd kernels/sgemm_gemmini_dma
./compile_virgo.sh
# compile GEMM kernels for tensor cores
cd ../sgemm_tcore
./compile_tcore.sh
# compile FlashAttention kernels
cd ../flash_attention
./compile_flash.sh
```

A.4.5 Compile simulation binaries. Exit to the root directory, then:

```
cd chipyard/sims/vcs
source ../../env.sh
# compile simulator binaries (~10 minutes)
./scripts/compile_designs.sh
```

A.5 Basic test

To check if everything worked up till this point, under `chipyard/sims/vcs`, run

```
./scripts/sanity.sh
```

You should see this output:

```
Sanity check passed!
```

A.6 Experiment workflow

A.6.1 Running RTL simulations. Ensure you are in a `tmux` or a screen session, as this step runs a long process. Under `chipyard/sims/vcs`:

```
source ../../env.sh
# start kernel runs
./scripts/run_sims.sh
```

We estimate that the longest simulation, i.e. 1024×1024 GEMM on the Volta configuration, will take around 24 to 30 hours. The script shows the current simulation timestamp in nanoseconds and clock rate in Hz; you should see a total of 14 concurrent simulations.

The subsequent steps require RTL simulation results. If you continue before all simulations are finished, their outputs may be partial.

A.6.2 Verifying hardware utilization. From chipyard/sims/vcs, run:

```
./scripts/utilization.sh > \
  ../../../../scripts/cycles.csv
./scripts/utilization.flash.sh > \
  ../../../../scripts/cycles.flash.csv
```

The script will process the microarchitectural trace logs generated from the RTL simulations, and print to the terminal the MAC utilization numbers that should match Table 3 for GEMM, and the “Performance & Utilization” paragraph in Section 6.2 for FlashAttention.

A.6.3 Reproducing power/energy measurements and plots. Back at the root directory outside chipyard, run:

```
cd scripts/
python run_plots.py
```

The script will output reproduced metrics along with the directions of how to link the metrics to figures and values in the paper. Please note that if the previous step of running RTL simulations is not finished, the generated plot might be missing some bars. Specifically, the 1024×1024 dimension GEMMs for Virgo and Ampere may take a long time (>30 hrs), and running the script before their completion may result in empty energy plots.

Please also note that due to licensing restrictions with the commercial PDK used for RTL synthesis, we do not provide methods for reproducing power and area measurements in the paper. Instead, we supply static CSV files, `power_*.csv` and `area_summary.csv`, that contain the power measurement data used as input for the post-processing scripts. However, because the cycle latency from RTL simulation is dynamically evaluated, the energy metrics will also be dynamically generated and evaluated by multiplying the power measurement with the cycle latency.

A.6.4 Verifying shared memory footprint metrics.

From chipyard/sims/vcs, run:

```
./scripts/smem_util.sh
```

The script will process the FSDB waveform files generated from the RTL simulation, and report the access footprint to the shared memory that shall match Table 4.

A.6.5 Software dependencies. The Vortex toolchain binaries provided in the artifact are built for an Ubuntu 20.04 LTS system or newer. Additionally, we find that Verilator fails to simulate our RTL due to crashes, and having access to the Synopsys VCS compiler is necessary for correct simulation. Our evaluation is tested with VCS version V-2023.12-SP1.

The post-processing and plotting scripts require a working Python 3 environment with following packages installed: `ripgrep`, `pandas`, `matplotlib`, `numpy`. These are used for generating input data for the kernel workloads, parsing log outputs, and generating plots. Setting up a Conda environment with these packages installed may be helpful.

A.7 Evaluation and expected results

We explain how the reproduced results link to the contents of the paper in the individual steps listed in Section A.6, and also in the terminal outputs from the scripts. With all of the above steps completed, we expect the following results to have been evaluated:

- Cycle execution latency and hardware utilization of the GPU running GEMM and FlashAttention kernels (Table 3 and Section 6.2),
- Power and energy measurements and plots for GEMM and FlashAttention (Section 6.1, 6.2, Figure 8–11)
- Shared memory footprint measurements (Table 4).

Specifically, the plots generated in Section A.6.3 correspond to the following figures in the paper:

- Figure 8: `fig-soc-power-energy-1x4.pdf`
- Figure 9: `fig-soc-power-breakdown.pdf`
- Figure 10: `fig-core-power-breakdown.pdf`
- Figure 11: `fig-matrix-unit-energy-breakdown.pdf`
- Figure 12: `fig-flash-power-energy-breakdown.pdf`

A.8 Methodology

Submission, reviewing and badging methodology:

- <https://www.acm.org/publications/policies/artifact-review-badging>
- <http://cTuning.org/ae/submission-20201122.html>
- <http://cTuning.org/ae/reviewing-20201122.html>

References

- [1] AMD. 2021. AMD CDNA 2 Architecture. <https://www.amd.com/content/dam/amd/en/documents/instinct-business-docs/white-papers/amd-cdna2-white-paper.pdf>.
- [2] AMD. 2024. AMD Matrix Instruction Calculator. https://github.com/ROCm/amd_matrix_instruction_calculator/blob/dae289b7f681776584749e3ae21f177b7f974d92/README.md.
- [3] AMD. 2024. Composable Kernel. https://github.com/ROCm/composable_kernel.
- [4] Alon Amid, David Biancolin, Abraham Gonzalez, Daniel Grubb, Sagar Karandikar, Harrison Liew, Albert Magyar, Howard Mao, Albert Ou, Nathan Pemberton, Paul Rigge, Colin Schmidt, John Wright, Jerry Zhao, Yakun Sophia Shao, Krste Asanović, and Borivoje Nikolić. 2020. Chippyard: Integrated design, simulation, and implementation framework for custom socs. *IEEE Micro* 40, 4 (2020).
- [5] Simran Arora, Sabri Eyuboglu, Michael Zhang, Aman Timalisina, Silas Alberti, Dylan Zinsley, James Zou, Atri Rudra, and Christopher Ré. 2024. Simple linear attention language models balance the recall-throughput tradeoff. arXiv:2402.18668 [cs.CL] <https://arxiv.org/abs/2402.18668>
- [6] Krste Asanović, Rimas Avizienis, Jonathan Bachrach, Scott Beamer, David Biancolin, Christopher Celio, Henry Cook, Daniel Dabbelt, John Hauser, Adam Izraelevitz, Sagar Karandikar, Ben Keller, Donggyu Kim, and John Koenig. 2016. The Rocket Chip Generator. *EECS Department, University of California, Berkeley, Tech. Rep. UCB/EECS-2016-17* 4 (2016).
- [7] Ganesh Bikshandi and Jay Shah. 2023. A Case Study in CUDA Kernel Fusion: Implementing FlashAttention-2 on NVIDIA Hopper Architecture using the CUTLASS Library. arXiv:2312.11918 [cs.LG] <https://arxiv.org/abs/2312.11918>
- [8] Robert A. Bridges, Neena Imam, and Tiffany M. Mintz. 2016. Understanding GPU power: A survey of profiling, modeling, and simulation methods. *ACM Computing Surveys (CSUR)* 49, 3 (2016).
- [9] Tom Brown, Benjamin Mann, Nick Ryder, Melanie Subbiah, Jared Kaplan, Prafulla Dhariwal, Arvind Neelakantan, Pranav Shyam, Girish Sastry, Amanda Askell, et al. 2020. Language models are few-shot learners. *Advances in neural information processing systems (NeurIPS)* (2020).
- [10] Jack Choquette. 2023. NVIDIA Hopper H100 GPU: Scaling Performance. *IEEE Micro* 43, 3 (2023), 9–17. doi:10.1109/MM.2023.3256796
- [11] Henry Cook. 2016. *Productive Design of Extensible On-Chip Memory Hierarchies*. Ph.D. Dissertation. EECS Department, University of California, Berkeley. <http://www2.eecs.berkeley.edu/Pubs/TechRpts/2016/EECS-2016-89.html>
- [12] Henry Cook, Wesley Terpstra, and Yunsup Lee. 2017. Diplomatic design patterns: A TileLink case study. In *1st Workshop on Computer Architecture Research with RISC-V*, Vol. 23.
- [13] NVIDIA Corporation. 2017. Nvidia Tesla V100 GPU architecture. <https://images.nvidia.com/content/volta-architecture/pdf/volta-architecture-whitepaper.pdf>.
- [14] NVIDIA Corporation. 2022. NVIDIA A100 Tensor Core GPU Datasheet. <https://www.nvidia.com/content/dam/en-zz/Solutions/Data-Center/a100/pdf/nvidia-a100-datasheet-nvidia-us-2188504-web.pdf>.
- [15] NVIDIA Corporation. 2024. NVIDIA Ampere GPU Architecture Tuning Guide. https://docs.nvidia.com/cuda/pdf/Ampere_Tuning_Guide.pdf.
- [16] NVIDIA Corporation. 2024. NVIDIA H100 Tensor Core GPU Datasheet. <https://resources.nvidia.com/en-us-tensor-core/nvidia-tensor-core-gpu-datasheet>.
- [17] NVIDIA Corporation. 2024. Parallel Thread Execution ISA Version 8.5. <https://docs.nvidia.com/cuda/parallel-thread-execution/index.html>.
- [18] Jack W. Davidson and Sanjay Jinturkar. 1994. Memory access coalescing: A technique for eliminating redundant memory accesses. *Acm Sigplan Notices* 29, 6 (1994).
- [19] Michael Davies, Ian McDougall, Selvaraj Anandaraj, Deep Machchhar, Rithik Jain, and Karthikeyan Sankaralingam. 2024. A Journey of a 1,000 Kernels Begins with a Single Step: A Retrospective of Deep Learning on GPUs. In *Proceedings of the International Conference on Architectural Support for Programming Languages and Operation Systems (ASPLOS)*.
- [20] Ruibo Fan, Wei Wang, and Xiaowen Chu. 2024. DTC-SpMM: Bridging the Gap in Accelerating General Sparse Matrix Multiplication with Tensor Cores. In *Proceedings of the International Conference on Architectural Support for Programming Languages and Operation Systems (ASPLOS)*.
- [21] Hasan Genc, Seah Kim, Alon Amid, Ameer Haj-Ali, Vignesh Iyer, Pranav Prakash, Jerry Zhao, Daniel Grubb, Harrison Liew, Howard Mao, Albert Ou, Colin Schmidt, Samuel Steffl, John Wright, Ion Stoica, Jonathan Ragan-Kelley, Krste Asanović, Borivoje Nikolic, and Yakun Sophia Shao. 2021. Gemmini: Enabling Systematic Deep-Learning Architecture Evaluation via Full-Stack Integration. In *Design Automation Conference*.
- [22] Guin Gilman, Samuel S. Ogden, Tian Guo, and Robert J. Walls. 2021. Demystifying the placement policies of the NVIDIA GPU thread block scheduler for concurrent kernels. *ACM SIGMETRICS Performance Evaluation Review* 48, 3 (2021).
- [23] John Hauser. 2019. Berkeley HardFloat. <http://www.jhauser.us/arithmetic/HardFloat.html>.
- [24] Miro Hodak, Masha Gorkovenko, and Ajay Dholakia. 2019. Towards power efficiency in deep learning on data center hardware. In *IEEE International Conference on Big Data (Big Data)*.
- [25] Guyue Huang, Zhengyang Wang, Po-An Tsai, Chen Zhang, Yufei Ding, and Yuan Xie. 2023. RM-STC: Row-Merge Dataflow Inspired GPU Sparse Tensor Core for Energy-Efficient Sparse Acceleration. In *Proceedings of the International Symposium on Microarchitecture (MICRO)*.
- [26] Intel. 2022. Introduction to the Xe-HPG Architecture. <https://www.intel.com/content/www/us/en/developer/articles/technical/introduction-to-the-xe-hpg-architecture.html>.
- [27] Sagar Karandikar, Howard Mao, Donggyu Kim, David Biancolin, Alon Amid, Dayeol Lee, Nathan Pemberton, Emmanuel Amaro, Colin Schmidt, Aditya Chopra, Qijing Huang, Kyle Kovacs, Borivoje Nikolic, Randy Katz, Jonathan Bachrach, and Krste Asanović. 2018. FireSim: FPGA-accelerated Cycle-exact Scale-out System Simulation in the Public Cloud. In *Proceedings of the International Symposium on Computer Architecture (ISCA)*.
- [28] Andrew Kerr, Duane Merrill, Julien Demouth, and John Tran. 2017. Cutlass: Fast linear algebra in cuda c++. *NVIDIA Developer Blog* (2017).
- [29] Hyeonjin Kim, Sungwoo Ahn, Yunho Oh, Bogil Kim, Won Woo Ro, and William J. Song. 2020. Duplo: Lifting redundant memory accesses of deep neural networks for GPU tensor cores. In *Proceedings of the International Symposium on Microarchitecture (MICRO)*.
- [30] Jae Seok Kwak, Myung Kuk Yoon, Ipoom Jeong, Seunghyun Jin, and Won Woo Ro. 2023. INTERPRET: Inter-Warp Register Reuse for GPU Tensor Core. In *Proceedings of the International Conference on Parallel Architectures and Compilation Techniques (PACT)*.
- [31] Baolin Li, Rohin Arora, Siddharth Samsi, Tirthak Patel, William Arcand, David Bestor, Chansup Byun, Rohan Basu Roy, Bill Bergeron, John Holodnak, et al. 2022. AI-enabling workloads on large-scale GPU-accelerated system: Characterization, opportunities, and implications. In *Proceedings of the International Symposium on High-Performance Computer Architecture (HPCA)*.
- [32] Weile Luo, Ruibo Fan, Zeyu Li, Dayou Du, Qiang Wang, and Xiaowen Chu. 2024. Benchmarking and Dissecting the Nvidia Hopper GPU Architecture. <https://arxiv.org/abs/2402.13499>. arXiv:2402.13499 [cs.AR]
- [33] Pratyush Patel, Zibo Gong, Syeda Rizvi, Esha Choukse, Pulkit Misra, Thomas Anderson, and Akshitha Sriraman. 2023. Towards improved power management in cloud gpus. *IEEE Computer Architecture Letters* 22, 2 (2023).

- [34] Md A. Raihan, Negar Goli, and Tor M. Aamodt. 2019. Modeling deep learning accelerator enabled gpus. In *Proceedings of the International Symposium on Performance Analysis of Systems and Software (ISPASS)*.
- [35] Gabin Schieffer, Daniel Medeiros, Jennifer Faj, Aniruddha Marathe, and Ivy Peng. 2024. *Characterizing the Performance, Power Efficiency, and Programmability of AMD Matrix Cores*. Technical Report. Lawrence Livermore National Laboratory, Livermore, CA.
- [36] Jaime Sevilla, Lennart Heim, Anson Ho, Tamay Besiroglu, Marius Hobbhahn, and Pablo Villalobos. 2022. Compute trends across three eras of machine learning. In *International Joint Conference on Neural Networks (IJCNN)*.
- [37] Jay Shah, Ganesh Bikshandi, Ying Zhang, Vijay Thakkar, Pradeep Ramani, and Tri Dao. 2024. FlashAttention-3: Fast and Accurate Attention with Asynchrony and Low-precision. arXiv:2407.08608 [cs.LG] <https://arxiv.org/abs/2407.08608>
- [38] James E. Smith. 1982. Decoupled access/execute computer architectures. *ACM SIGARCH Computer Architecture News* 10, 3 (1982).
- [39] Wei Sun, Ang Li, Tong Geng, Sander Stuijk, and Henk Corporaal. 2022. Dissecting tensor cores via microbenchmarks: Latency, throughput and numeric behaviors. *IEEE Transactions on Parallel and Distributed Systems* 34, 1 (2022).
- [40] Seunghwan Sung, Sujin Hur, Sungwoo Kim, Dongho Ha, Yunho Oh, and Won Woo Ro. 2023. MAD MACce: Supporting Multiply-Add Operations for Democratizing Matrix-Multiplication Accelerators. In *Proceedings of the International Symposium on Microarchitecture (MICRO)*.
- [41] Guangming Tan, Linchuan Li, Sean Triechele, Everett Phillips, Yungang Bao, and Ninghui Sun. 2011. Fast implementation of DGEMM on Fermi GPU. In *Proceedings of 2011 International Conference for High Performance Computing, Networking, Storage and Analysis*.
- [42] Blaise Tine, Krishna Praveen Yalamarthy, Fares Elsabbagh, and Hye-soon Kim. 2021. Vortex: Extending the RISC-V ISA for GPGPU and 3D-graphics. In *Proceedings of the International Symposium on Microarchitecture (MICRO)*.
- [43] Jiajun Wang, Ahmed Khawaja, George Biros, Andreas Gerstlauer, and Lizy K John. 2016. Optimizing GPGPU kernel summation for performance and energy efficiency. In *45th International Conference on Parallel Processing Workshops (ICPPW)*.
- [44] Yang Wang, Chen Zhang, Zhiqiang Xie, Cong Guo, Yunxin Liu, and Jingwen Leng. 2021. Dual-side sparse tensor core. In *Proceedings of the International Symposium on Computer Architecture (ISCA)*.
- [45] Da Yan, Wei Wang, and Xiaowen Chu. 2020. Demystifying tensor cores to optimize half-precision matrix multiply. In *Proceedings of the International Parallel and Distributed Processing Symposium*.
- [46] Michael Zhang, Kush Bhatia, Hermann Kumbong, and Christopher Ré. 2024. The hedgehog & the porcupine: Expressive linear attentions with softmax mimicry. arXiv:2402.04347 [cs.LG] <https://arxiv.org/abs/2402.04347>
- [47] Xiuxia Zhang, Guangming Tan, Shuangbai Xue, Jiajia Li, Keren Zhou, and Mingyu Chen. 2017. Understanding the GPU microarchitecture to achieve bare-metal performance tuning. In *Proceedings of the Symposium on Principles and Practice of Parallel Programming (PPoPP)*.
- [48] Yunan Zhang, Po-An Tsai, and Hung-Wei Tseng. 2022. SIMD2: A generalized matrix instruction set for accelerating tensor computation beyond GEMM. In *Proceedings of the International Symposium on Computer Architecture (ISCA)*.
- [49] Dan Zhao, Siddharth Samsi, Joseph McDonald, Baolin Li, David Bestor, Michael Jones, Devesh Tiwari, and Vijay Gadepally. 2023. Sustainable Supercomputing for AI: GPU Power Capping at HPC Scale. In *Proceedings of the 2023 ACM Symposium on Cloud Computing*.